Arch. Mech., **63**, 2, pp. 99–116, Warszawa 2011

Modelling of plasma formation during nanosecond laser ablation

T. MOŚCICKI, J. HOFFMAN, Z. SZYMAŃSKI

Institute of Fundamental Technological Research
Polish Academy of Science
Pawińskiego 5B
02-106 Warszawa, Poland
e-mail: tmosc@ippt.gov.pl

The interaction of laser beam with a target and next with the evaporated material is studied theoretically. In the case of a nanosecond laser pulse with 1064 nm wavelength, the ablation is thermal and therefore the interaction of the laser beam with a target is studied with the use of thermal model. The model which describes both the target heating, formation of the plasma and its expansion consists of equations of conservation of mass, momentum and energy and is solved with the use of Fluent software package. The calculations show a sharp increase of the plume temperature and pressure after plasma formation and following it, a considerable increase of the velocity of plasma plume. Maximum plasma pressure of 2×10^8 Pa, temperature of 61 500 K and front velocity of 3.8×10^4 $\mathrm{m \cdot s^{-1}}$ have been found. The results show that the Mie absorption cannot be neglected in the phase of plasma formation. The shape of the plume and plasma front velocity obtained from the model are close to that observed in the experiment carried out in similar conditions.*)

Key words: laser ablation, plasma formation, plasma expansion.

Copyright © 2011 by IPPT PAN

1. Introduction

Laser ablation is a well-established method of removing material from a solid surface by irradiating it with a laser beam. Applications include laser machining (drilling, engraving), cleaning contaminated surfaces (removal of paint or coating), deposition of thin coatings on different materials, production of new nanomaterials such as carbon nanotubes etc.

During laser ablation, the material evaporated from the target forms a thin layer of very dense plume, consisting of electrons, ions and neutrals. This plasma plume absorbs energy from the laser beam (by means of photoionization and inverse Bremsstrahlung) and its temperature and pressure grow. The resulting pressure gradient accelerates the plume to high velocity perpendicular to the target.

*)The paper was presented at 19th Polish National Fluid Dynamics Conference (KKMP), Poznań, 5–9.09.2010.

In this paper, theoretical modelling of the target heating and plasma formation during interaction with nanosecond laser pulse is presented. The set of equations consists of equation of conservation of mass, momentum and energy and is solved with the use of Fluent software package.

The mechanism of plasma formation and expansion consists of three stages. During the interaction of the laser beam with a material, the target is heated to a temperature exceeding its boiling temperature and sometimes, also its critical temperature. The temperature to which the target is heated depends on the mechanism of interaction of the laser beam with the material. When the absorbed laser energy is transformed into heat, thermal ablation occurs. The second type of interaction called photochemical ablation takes place, when the quantum energy of the laser radiation is high enough to break inter-atomic bonds and desorbs particles from the surface [1]. In the case of an Nd:YAG laser with a wavelength of 1064 nm, the energy of quanta is only 1.16 eV and it can be assumed that the photochemical absorption is negligible.

The characteristic time of the target temperature rise varies from 1 nanosecond in the case of dielectrics, to some tens of nanoseconds in the case of metals [1]. At the same moment, the process of ablation begins. In the second stage, the ablated particles are heated by the laser beam to temperatures of up to several tens of kilokelvins and form a plasma plume. The characteristic time of plasma heating is 10–100 nanoseconds depending on the intensity of the laser beam and quantum energy [2]. Next, the laser pulse terminates and plasma plume expands adiabatically.

All these phases are studied theoretically in this paper. The aluminium target is ablated by a Nd:YAG laser working at its fundamental wavelength of 1064 nm with 10 ns (FWHM – Full Width at Half Maximum) pulse duration. Aluminum is chosen because its all necessary material functions are available and comparison with some other theoretical results is possible. In addition, aluminium or aluminium/titanium multilayer coatings are used to improve corrosion resistance of magnesium alloys, which draw more and more interest in electronic equipment, automotive and aerospace industry.

The emphasis is put on mechanisms of plasma formation and the plasma plume velocity. The material evaporation is strongly affected by the plasma formation and consequently depends on the absorption coefficient of laser radiation in plasma. The dense plasma plume can entirely block laser radiation and subsequently, the energy transfer from the laser beam to the material. Even if the width of a laser pulse is 20 ns, the relevant laser-target interaction is only during the first 10 ns. Further the laser radiation is blocked by developing plasma plume. This dense plasma absorbs energy from the laser beam and its temperature and pressure grow. The thickness of the plasma layer is small compared to its other dimensions, therefore the pressure gradient inside the major part of this layer

is large and nearly perpendicular to the surface. Such pressure gradient accelerates the plume to high velocity perpendicular to the target. However, plume velocities observed in experiments are much higher than those resulting from the existing theoretical models [3, 4]. Such high velocities were attributed to the acceleration of ions in the electrostatic field created by photo- and thermionic electron emission, next followed by ejection of positive ions, but the theoretical description of this effect did not confirm high velocity increase [5]. Recently, Tan *et al.* [6] developed a model, which led to plume velocities as high as observed in the experiments. However, their mixed analytical-numerical model is based on many assumptions and therefore is of limited validity. The model developed in this paper is similar to those used in [7, 8] and is free from unnecessary assumptions.

2. Theoretical model

2.1. Initial assumptions

We adopt here the following model of the investigated phenomenon: a high energy, short duration laser pulse is focused on a small area of the surface of a solid aluminium target. This results in melting and evaporation of some portion of the target material. The stream of ablated particles is directed perpendicularly to the target surface. Further interaction of the laser beam with the ablated material results in producing a small volume of very dense plasma. The laser is an Nd:YAG laser operating at its fundamental wavelength of 1064 nm with a pulse energy of 450 mJ and 10 ns pulse duration. The laser beam is focused on aluminium target to a diameter of 2.4 mm, which results in the laser fluence of $\sim$10 $\mathrm{J \cdot cm^{-2}}$ (intensity $I_L = 1\ \mathrm{GW \cdot cm^{-2}}$). The plasma expands into ambient air at a pressure of 1 Pa. In the case of a nanosecond laser, the ablation is thermal and hence the initial conditions for plume expansion may be described as follows.

The particles released from the target have half-maxwellian velocity distribution – they can move only forward. The full maxwellian distribution is reached after some collisions between particles in the Knudsen layer, whose thickness is of the order of a few mean free paths. The vapour density ρ_v, the pressure p_v and the temperature T_v at the end of the Knudsen layer depend on the Mach number only [9]. If vapour velocity equals sonic speed a then the parameters are $T_v \sim 0.67T_s$, $p_v \sim 0.21p_s$, $\rho_v \sim 0.31\rho_s$ (for monoatomic vapour), where the subscript s denotes the surface [9]. These values are taken as initial conditions for further calculations. The temperature T_s is determined solving heat transfer equation and the pressure p_s is calculated from the Clausius–Clapeyron equation [9]. At the end of the Knudsen layer, the particles have

macroscopic flow velocity $v_0 = a = (\gamma k_B T_v/m)^{0.5}$ perpendicular to the target surface.

2.2. Target heating

An enthalpy-porosity technique is used in Fluent [10] for modeling the solidification/melting process. In this technique, the melt interface is not tracked explicitly. Instead, a quantity called the liquid fraction, which indicates the fraction of the cell volume that is in liquid form, is associated with each cell in the domain. The liquid fraction is computed at each iteration, based on an enthalpy balance [10]. The energy equation is written as

$$\frac{\partial(\rho H)}{\partial t} + \operatorname{div}(\rho \mathbf{v} H) = \operatorname{div}(k \nabla T), \tag{2.1}$$

where ρ is the mass density, $\mathbf{v} = \mathbf{v}_c + \mathbf{u}$, where $\mathbf{v}_c$ is the convection velocity and $\mathbf{u}$ is the recession velocity (Eq. (2.3)), k is the thermal conductivity, and T is the temperature. $H = \int_{T_0}^{T} c_p dT + f_l L_m$, where c_p is the specific heat at constant pressure, L_m is the latent heat of melting and the liquid fraction f_l is defined as 0 for $T < T_{\text{sol}}$, 1 for $T_{\text{liq}} < T$ and $f_l = (T - T_{\text{sol}})/(T_{\text{liq}} - T_{\text{sol}})$ if $T_{\text{sol}} < T < T_{\text{liq}}$. T_{sol} and T_{liq} denote the solidus and liquidus temperature, respectively.

The boundary condition at the place where the laser beam strikes the surface is

$$-k\frac{\partial T_s}{\partial \mathbf{n}} = I_L \cdot A - \rho u(t) L_v, \tag{2.2}$$

where I_L is the laser intensity, A is the surface absorptivity, L_v is the latent heat of vaporization and $\mathbf{n}$ is the unit vector perpendicular to the surface. Energy losses due to thermal radiation from the surface are small compared to other terms and have been neglected. At other boundaries $T = 300$ K is assumed.

Under the assumptions mentioned above it can be assumed that the vaporization rate $\rho \cdot u(t)$ is given by the Hertz–Knudsen equation and the vapor pressure above the vaporized surface results from the Clausius–Clapeyron equation [11]. Then

$$u(t) = (1-\beta)\frac{p_b}{\rho}\left(\frac{m}{2\pi k_B T_s}\right)^{1/2} \exp\left[\frac{L_v}{k_B}\left(\frac{1}{T_b} - \frac{1}{T_s}\right)\right], \tag{2.3}$$

where k_B is the Boltzmann constant, T_s is the surface temperature, T_b is the boiling temperature under a reference pressure p_b, and β is the fraction of the vaporized particles returning to the target surface (back flux). For stationary vaporization $\beta = 0.18$. $u(t)$ is included in Eq. (2.1) using User Defined Function [10].

Other aluminium properties were as follows [12]; latent heat of melting $L_m = 397 \times 10^3$ J/kg, latent heat of vaporization $L_v = 10.75 \times 10^6$ J/kg, liquidus temperature $T_{\text{liq}} = 933$ K, solidus temperature $T_{\text{sol}} = 934$ K and the boiling temperature $T_b = 2720$ K. Absorptivity of the laser radiation by aluminium target surface was assumed to be 0.2 [8].

The energy source term I_L was used in the form which fits the shape of the laser pulse used in our laboratory

$$I_L(t,r) = \frac{CF}{\tau} \exp\left(-\left(\frac{t-t_0}{\tau}\right)^2\right)\left(1-\left(\frac{r}{w}\right)^2\right) \times \exp\left(-\int \kappa dz\right), \tag{2.4}$$

where F is the laser fluence, τ is the laser pulse duration, w is the beam radius, κ is the plasma absorption coefficient, r and z are radial and axial coordinates, respectively, and the integration is over the distance travelled by the beam. The numerical factor C results from normalization, t_0 is the time offset of the beam maximum intensity. The first part of the Eq. (2.4) describes temporal evolution of the laser intensity, the second parabolic energy distribution in the laser beam and the last exponential component takes into account the attenuation of the laser beam on its way to the point (r, z).

2.3. Absorption of the laser beam

The plasma absorption coefficient κ can be determined when plasma parameters are known. All possible absorption mechanisms: the electron-atom inverse Bremsstrahlung, the electron-ion inverse Bremsstrahlung, photoionization and the Mie absorption were taken into account. The absorption coefficient depends on the composition of the plume i.e. the concentration of neutral and ionized particles, plume temperature and the laser wavelength. The composition of the plume depends on gas pressure and temperature and was calculated assuming the local thermodynamic equilibrium, i.e. the composition of the plasma at a given temperature and pressure were determined by the state equation, the Dalton law, the set of the Saha equations and the condition of electrical neutrality.

The total continuous absorption coefficient can be written as

$$\kappa = \sum_{\lambda} \left(\kappa_{ff}^{ei}(\lambda) + \kappa_{fb}(\lambda) + \kappa_{ff}^{ea}(\lambda)\right) \times \left[1 - \exp\left(-\frac{hc}{\lambda kT}\right)\right], \tag{2.5}$$

where indices *fb* and *ff* denote free-bound and free-free transitions i.e. the absorption due to the photoionisation and inverse Bremsstrahlung, respectively, and *ei* and *ea* denote electron-ion and electron-atom collisions. The last bracket contains contribution from the stimulated emission. Formulas for κ_{fb} and κ_{ff}^{ei} were taken from [13] and those for k_{ff}^{ea} from [14] and are written below (in SI units):

$$\kappa^{fb}(\lambda) = \frac{32\pi^2 k_B}{3\sqrt{3}c_0 h^4}\left(\frac{e_0^2}{4\pi\varepsilon_0}\right)^3 \sum_z z^2 n_{z-1}\cdot\frac{g_{z,1}}{U_{z-1}}\frac{T_e\lambda^3}{c_0^3} \times \exp\left\{-\frac{E_j}{k_B T_e}\right\}\left(\exp\left\{\frac{h\nu}{k_B T_e}\right\}-1\right)\cdot\xi(T_e,\lambda), \tag{2.6}$$

$$\kappa_{ei}^{ff}(\lambda) = \frac{8\pi\cdot e_0^6}{3m_e hc(6\pi m_e k_B)^{1/2}(4\pi\varepsilon_0)}\cdot\lambda^3\cdot n_e T^{-1/2}\times\sum_{z=1} z^2 n_z\cdot G_{ff}, \tag{2.7}$$

$$\kappa_{ea}(\lambda) = \frac{16e_0^2\lambda^3}{3(4\pi\varepsilon_0)\cdot c^4 h}\left(\frac{k}{2\pi m_e}\right)^{3/2} n_a n_e T^{3/2} \times\sigma_{ea}(T)\cdot\left[1+\left(1+\frac{hc}{\lambda k_B T}\right)^2\right], \tag{2.8}$$

where n_{z-1} is the density of parent atom (or ion) $n_0 \equiv n_a$, n_e and n_z are the electron and ion density, respectively, T_e is the electron temperature, z denotes ion charge seen by free electron, $U_{z-1}(T)$ is the partition function, E_j is the ionization energy, g_z is the statistical weight of the parent ion, $\xi^{fb}(T_e,\lambda)$ is the Biberman factor, and G_{ff} is the Gaunt factor. Gaunt factors were taken from [15]. The electron-atom scattering cross-section σ_{ea} for aluminium was taken from [16].

The photoionization formula (2.6) has been derived for hydrogen-like atoms ($\xi^{fb}(T_e,\lambda)=1$) and the ξ-factor introduces the edge structure of the real coefficients. Its calculation necessitates the knowledge of photoionization cross-section. However, for longer wavelengths ξ goes to unity. Therefore in our calculations for 1064 nm $\xi = 1$ has been assumed. Our values of the absorption coefficient in the aluminium plasma without the Mie absorption are similar to those obtained in [8] though our values are by about 10% smaller.

The Mie absorption coefficient is equal to

$$\kappa_{\text{Mie}} = n_{cl}\sigma_{\text{Mie}}, \tag{2.9}$$

where n_{cl} is the number density of clusters and σ_{Mie} is the Mie absorption cross-section given by [17]

$$\sigma_{\text{Mie}} = \frac{8\pi^2 a^3}{\lambda}\text{Im}\left(\frac{\bar{n}^2-1}{\bar{n}^2+2}\right), \tag{2.10}$$

where a is the radius of spherical clusters, $\bar{n}$ is the complex refractive index of the clusters and λ is the wavelength of laser radiation. The data necessary to calculation were taken from [18]. Details of calculations of n_{cl} can be found in [19].

The results are shown in Fig. 1.

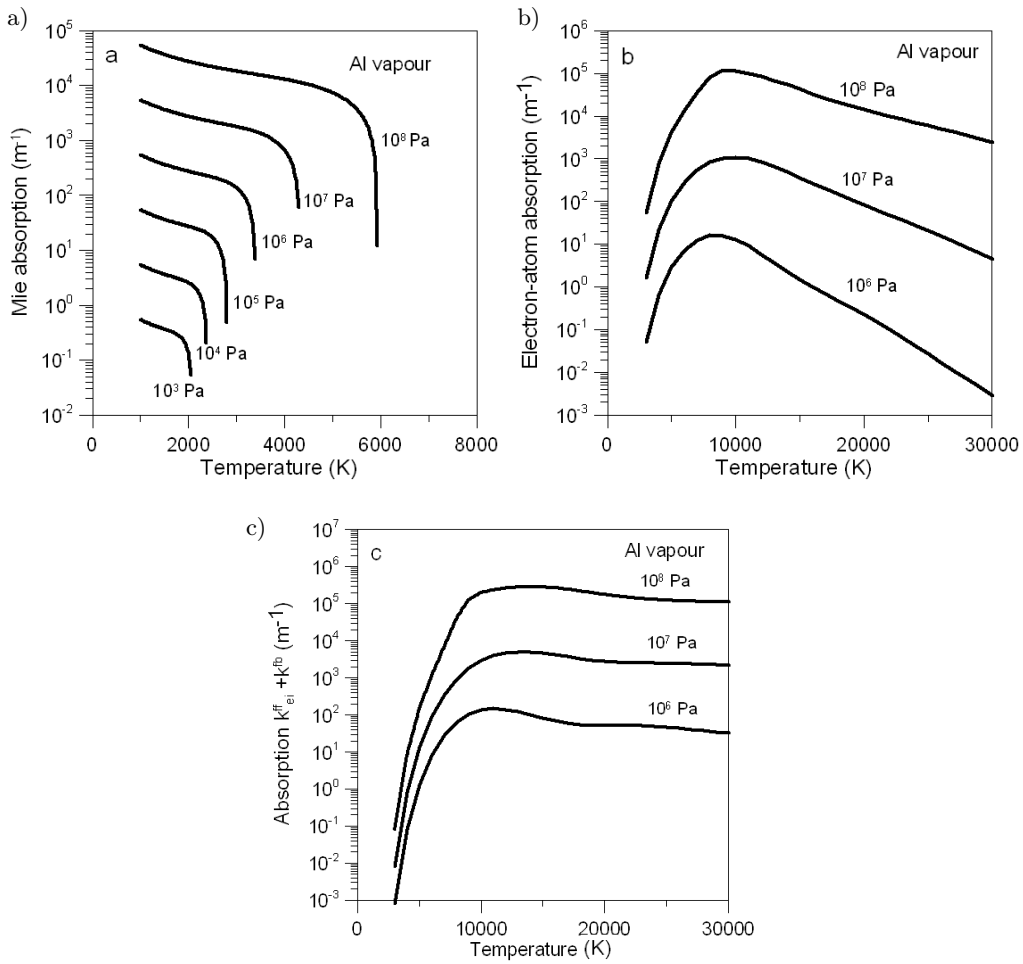

Fig. 1. Absorption of 1064 nm laser radiation in aluminium vapour; a) Mie absorption, b) electron-atom absorption, c) absorption due to Bremsstrahlung and photoionization.

2.4. Plume expansion

During the first few hundreds of nanoseconds after beginning of the laser pulse, the plasma is so dense that it can be treated as continuum fluid and equations of gasdynamics can be applied for its description. The plasma expansion model was solved in axial symmetry with the use of Fluent software package [10]. The set of equations used by Fluent consists of equation of conservation of mass, energy, momentum and a convection-diffusion equation in the form:

$$\frac{\partial \rho}{\partial t} + \nabla \cdot (\rho \mathbf{v}) = 0, \tag{2.11}$$

$$\frac{\partial}{\partial t}(\rho E) + \nabla \cdot (\mathbf{v}(\rho E + p)) = \kappa \cdot I_L - R, \tag{2.12}$$

$$\frac{\partial}{\partial t}(\rho \mathbf{v}) + \nabla \cdot (\rho \mathbf{v}\mathbf{v}) = -\nabla p + \rho \mathbf{g}, \tag{2.13}$$

$$\frac{\partial}{\partial t}(\rho Y_i) + \nabla \cdot (\rho \mathbf{v} Y_i) = 0, \tag{2.14}$$

where

$$Y_i = \frac{\rho_i}{\rho_i + \rho_k}, \tag{2.15}$$

E is energy $E = h - p/\rho + 0.5v^2$, h enthalpy $h = \sum_j Y_j h_j$, $h_j = \int_{T_{\mathrm{ref}}}^{T} c_{p,j} dT$, p – the pressure, Y_i – the mass fraction of ablated vapour in the gas mixture, $\mathbf{v}$ – the velocity vector, κ – the absorption coefficient of laser radiation, I_L – the laser intensity, R – the radiation loss function, $\mathbf{g}$ – the gravity.

In the first phase of the plume expansion, the gasdynamic effects prevail over transport phenomena and the momentum equation can be used in the Euler form. The coupled solver has been applied and hence only the convection component is included in the diffusion equation.

The mass density and the specific heat of aluminium vapour were calculated in all necessary range of pressures assuming the local thermodynamic equilibrium and taking into account the consecutive ionizations stages. The partition functions were taken from [20].

The source term including the interaction of a laser beam with the plasma plume $\kappa \cdot I_L$, (where I_L is given by Eq. (2.4)) and radiation losses R, was inserted into the program. The radiation losses R were calculated integrating the continuum emission coefficients over all wavelength (frequencies). The radiation of spectral lines has been neglected. The emission coefficients are not presented here because they can be obtained from the absorption coefficients given below using the Kirchhoff law, which connects the emission coefficient ε_λ with the absorption coefficient κ [13]:

$$\kappa = \varepsilon_\lambda / B_\lambda(T) \times \left(1 - \exp\left(-\frac{hc}{\lambda k_B T}\right)\right)^{-1}. \tag{2.16}$$

All the material functions depend on the temperature, pressure and mass fraction. This created a problem because the dependence of the specific heat on both the pressure and temperature is not envisaged in Fluent solver for compressible flow. Therefore the proper values of c_p had to be inserted to the program in successive time steps. In addition, the solver calculates the density from the equation of the ideal gas in the form

$$\rho = \frac{m \cdot p}{R_g T}, \tag{2.17}$$

where m is the atomic mass and R_g is the gas constant. Such a formulation does not take into account the change of density due to practically weightless electrons which appear in the ionization process. This problem was overcome by changing the atomic mass in order to get proper density values at high temperatures. Some iterations were necessary to obtain final results.

The assumption of local thermodynamic equilibrium is fulfilled, at least in the considered time span. The criterion for LTE has the form [13]

$$N_e \geq N_e^{\mathrm{cr}} = 1.6 \times 10^{18} T_e^{1/2} (\Delta E)^3, \tag{2.18}$$

where N_e^{cr} is the critical electron density (in m^{-3}) necessary to fulfil LTE conditions, T_e is the electron temperature (in K), and ΔE is the largest energy gap of atomic (ionic) energy level system (in eV). Since the largest energy gap for the Al I – Al III system is 7.73 eV, the electron density necessary to fulfil the above criterion is 1.8×10^{23} m^{-3} at a temperature of 60 000 K, which is typical for the plasma plume close to the target (at early stage of formation i.e. ∼100 ns from the laser pulse). Typical plasma density at this time is about one order higher. Since the relaxation time for establishment of LTE is about 1×10^{-11} s, transient phenomena should not disturb the equilibrium.

The assumption of one temperature is less reliable. The energy of the laser beam is supplied to electrons. Thus the electron temperature T_e will always exceed the temperature of heavy particles T_h: atoms and ions. The electrons transfer part of energy in elastic collisions with heavy particles and in inelastic collisions – mainly in ionizing collisions. The estimations show that the term describing the energy transfer in elastic collisions is by a factor of $(T_e - T_h) \times 10^{-4}$ smaller than the energy source term $\kappa \cdot I_L$. On the other hand, the term describing electron energy loss due to ionizing collisions is of the same order as the source term. This term together with excitation collision term can therefore diminish the temperature difference between the electrons and heavy particles to a few thousand kelvins. Above considerations concern the heating phase which takes place during 14–20 ns (see Section 3). After the cessation of the laser pulse, the equilibration of temperatures takes place within 1 ns.

The calculation domain was $r = 1.5$ cm and $z = 5$ cm with nonuniform grid with 70×210 nodes. The smallest computational cells had dimension of 0.1 mm × 0.1 μm at the target surface. They were fit to appearing gradients after preliminary calculations and it was checked that further decreasing of cell dimensions did not change the results.

The time step was adjusted to the smallest cells.

The boundary conditions for the above system of equations were as follows. The stream of aluminium vapour was directed perpendicularly to the target surface. The inlet temperature, velocity and pressure of ablated particles was calculated according to the target temperature and conditions at the end of

the Knudsen layer. At the wall the no-slip boundary and a fixed temperature condition were applied. At the outflow boundary, the pressure outlet boundary conditions [10] were used, which required the specification of a static pressure at the outlet boundary. This static pressure value is relative to the operating pressure. The axis boundary conditions were used at the centerline of the axis-symmetric geometry [10].

The above system of equations was solved iteratively. The target temperature was calculated and then the stream of ablated particles was determined at the end of the Knudsen layer. These conditions were taken as inlet conditions for plume expansion. Then the absorption of the laser radiation in developing plasma plume was determined and the target temperature was recalculated according to actual laser intensity at the target surface. The new target temperature was used to determine the conditions at the end of the Knudsen layer, which were subsequently used as inlet conditions for plume expansion. The applied method of modeling was tested by comparing the results for the ablation obtained in the same conditions as the results reported in [8]. Good agreement with the results of Mazhukin *et al.* was obtained.

3. Results

The target temperature as a function of time together with undisturbed laser intensity is shown in Fig. 2. The target maximum temperature reaches 7360 K at the axis centre at $t = 15$ nanosecond after the beginning of the laser pulse. At the same moment, plasma plume forms ahead of the target and then laser intensity practically drops to zero within a few nanoseconds. From this time on,

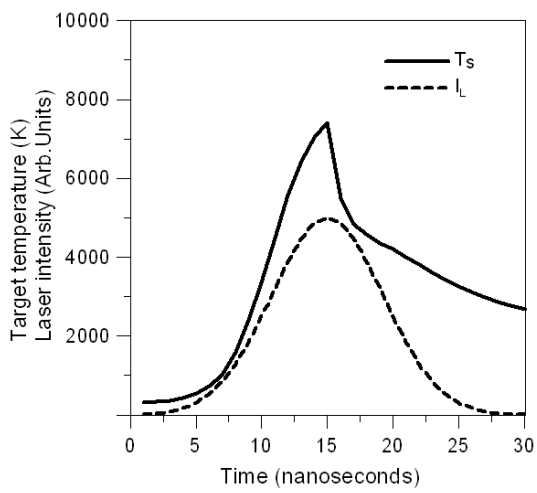

Fig. 2. Target temperature T_s and laser intensity I_L during first 30 nanoseconds (at $r = 0$).

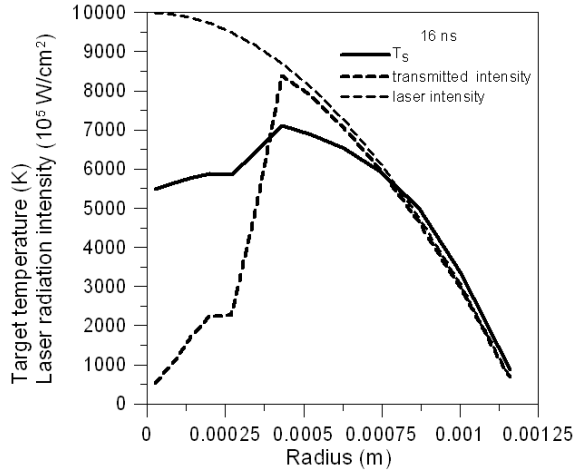

Fig. 3. Radial distribution of target temperature and transmitted laser intensity at $t = 16$ ns after the beginning of the laser pulse.

the target cools down. The radial distribution of the target temperature and transmitted laser radiation at $t = 16$ ns after the laser pulse is shown in Fig. 3.

Figure 4 shows the saturated vapour pressure p_s over the target surface and the plasma pressure p_p at the centreline. (Plasma parameters denote the parameters after the Knudsen layer). The saturated vapour pressure reaches 3.3×10^8 Pa, 15 nanoseconds from the beginning of the laser pulse. Up to 14-th nanosecond the plasma pressure p_p follows the relation resulting from the theory

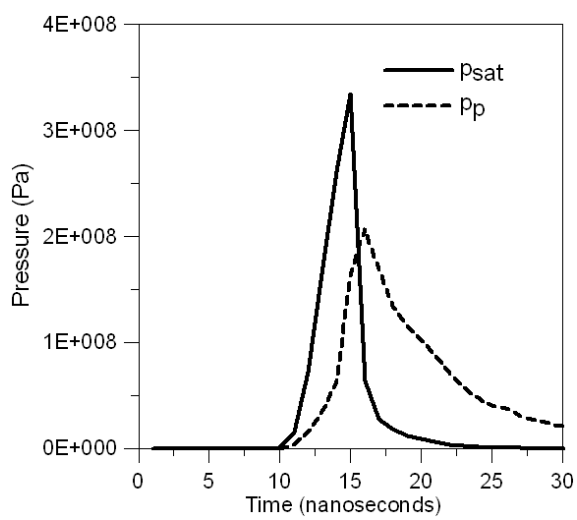

Fig. 4. Saturated vapour pressure p_{sat} and plasma pressure p_p during the first 30 ns (at $r = 0$).

of the Knudsen layer – $p_p = 0.21 \times p_{\text{sat}}$. Then the absorption of the laser beam starts abruptly and the plasma pressure grows rapidly and reaches 2.07×10^8 Pa at $t = 16$ ns. The plasma maximum density is reached at the same moment. The plasma temperature grows up to its maximum value of 61 500 K somewhat later at the 23-d nanosecond (Fig. 5). The plasma velocity increases even slower and reaches maximum value of 3.8×10^4 $\text{m} \cdot \text{s}^{-1}$ after 40 ns (see Fig. 6). Further the plume velocity slowly decreases due to interaction with the residual air.

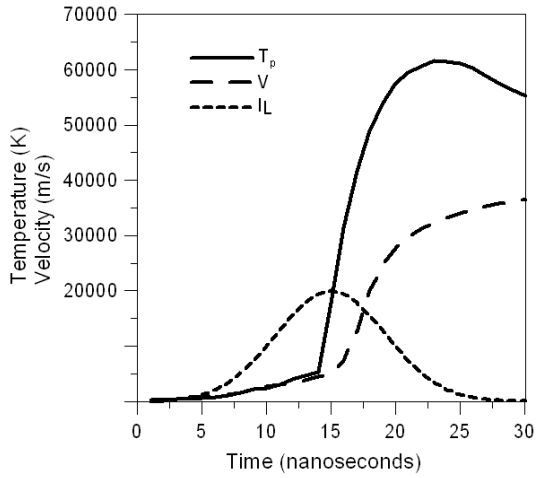

Fig. 5. Plasma temperature T_p and plasma velocity v at $r = 0$ during the first 30 nanoseconds (at $r = 0$).

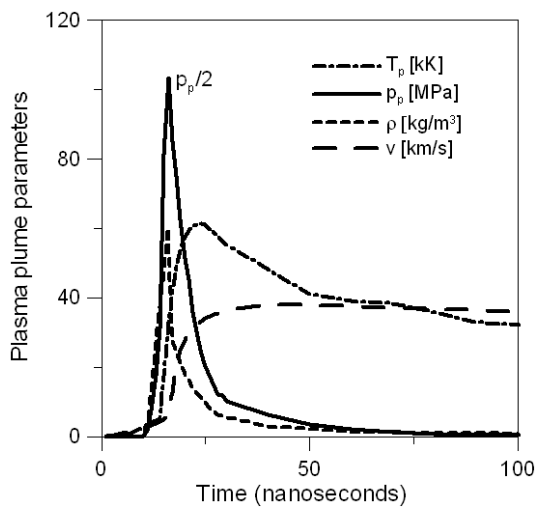

Fig. 6. Plasma parameters during 100 ns after the beginning of the laser pulse (at $r = 0$).

In Fig. 7 the effect of the Mie absorption on plasma temperature is shown. This kind of absorption analysed in [19] was neglected in other models [7, 8]. As we can see, its effect on the plasma temperature is considerable; without the Mie absorption the maximum plasma temperature and pressure are much lower; the temperature about 14 000 K, and the pressure about the factor of 1.6. This results from the fact that the Mie absorption is, in the case of aluminium, a dominant absorption mechanism in temperatures below 5000 K. The target temperature does not change significantly because in the case when the Mie absorption is neglected, the plasma which blocks the laser radiation develops merely two nanoseconds later when the target temperature is already decreasing. In other words, the Mie absorption results in faster plasma ignition (about 2 ns) and subsequent higher plasma temperatures are consequences of this faster ignition. Since the whole process is highly nonlinear, it is very difficult to estimate the effect of possible uncertainties of the Mie absorption coefficient on the resulting plasma temperatures. However, uncertainties in the Mie absorption coefficient lie in the values of complex refractive index in high temperatures which was estimated within 5% [18].

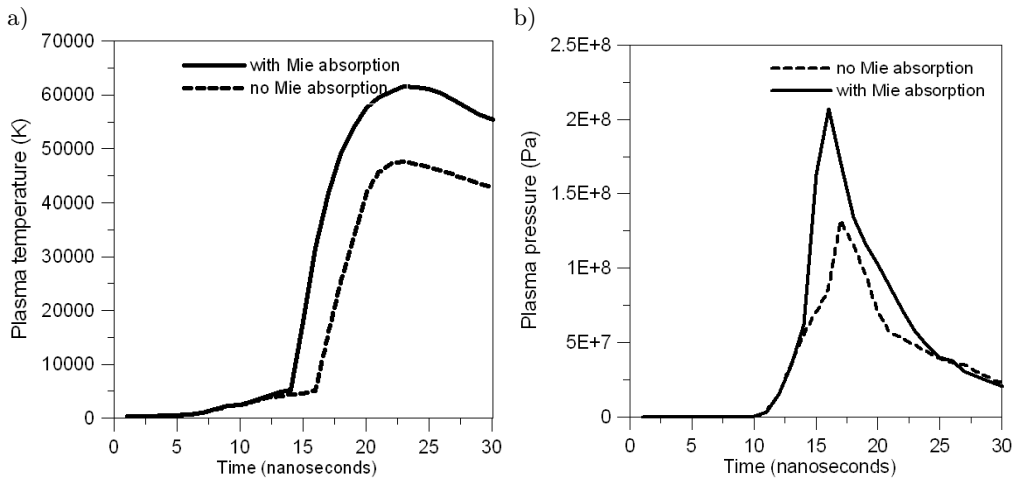

Fig. 7. Effect of the Mie absorption on plasma temperature (a) and pressure (b) at $r = 0$.

In Fig. 8 the distributions of the plume temperature, pressure, density and velocity are shown at a time $t = 50$ ns after the beginning of the laser pulse. The plasma maximum temperature is now 42 000 K, the plasma pressure 6×10^6 Pa, and the front velocity 3.8×10^4 m $\cdot$ s^{-1}. Mixing with the ambient air occurs only in a narrow outer region and hence it is insignificant.

After 100 ns (see Fig. 9) of expansion the plasma dimensions are considerably bigger while the pressure and temperature decreases. These values continue to decrease during further plasma expansion. After 100 ns the plasma front velocity

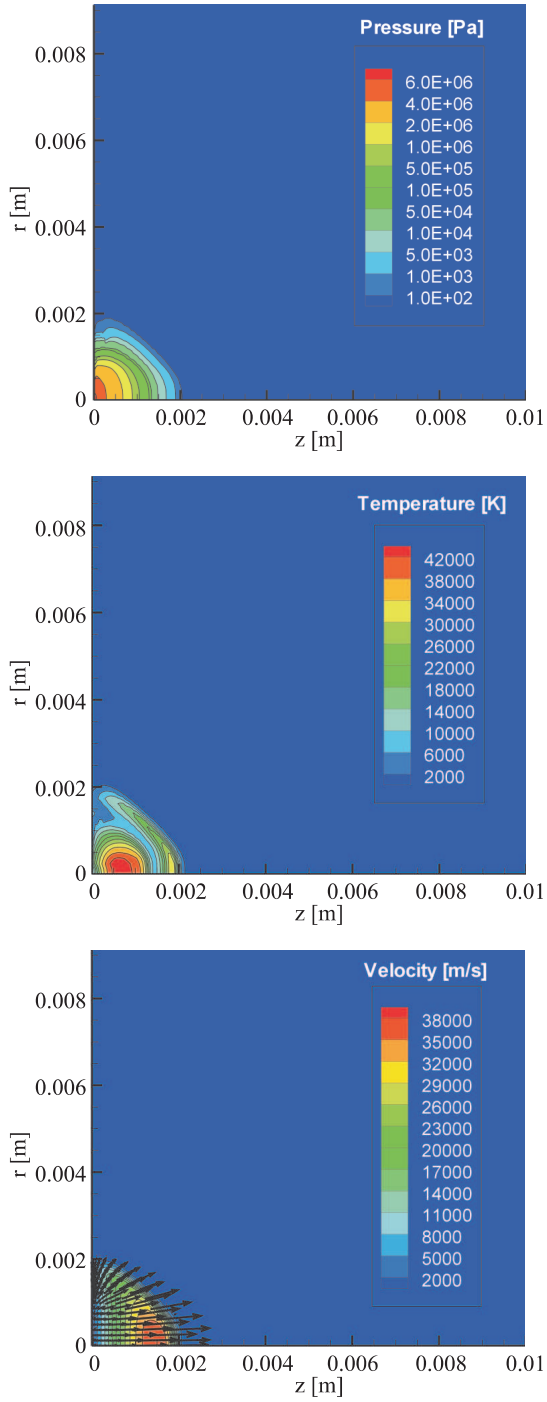

Fig. 8. Distribution of pressure, temperature and velocity in plasma induced during laser ablation of aluminium, 50 ns after the beginning of the laser pulde.

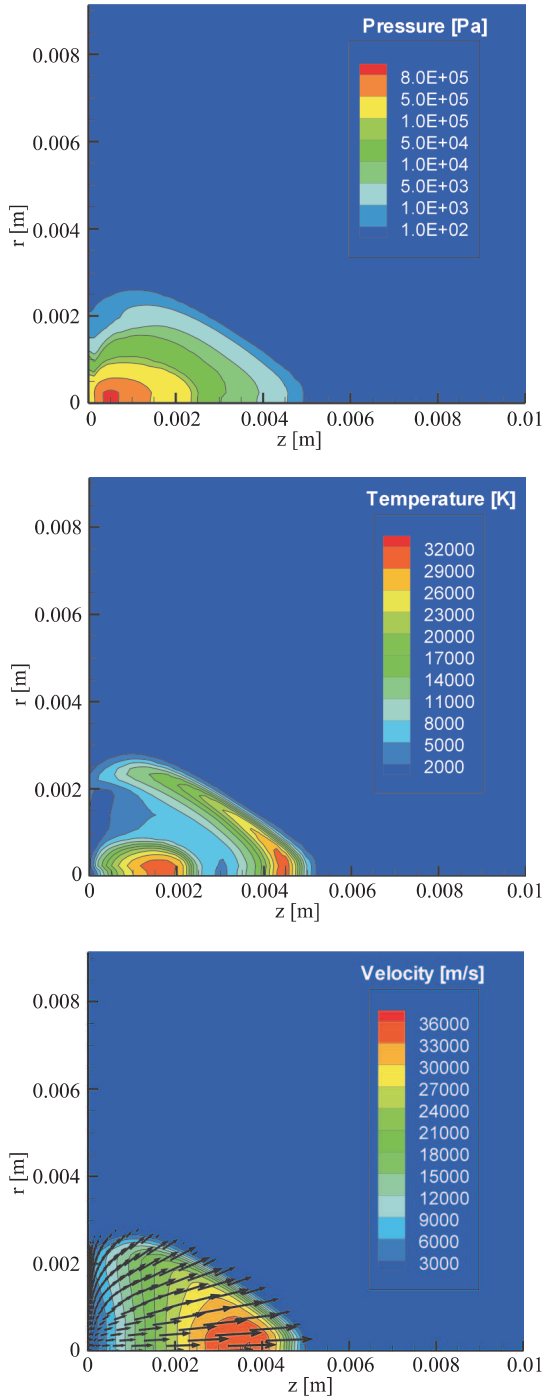

Fig. 9. Distribution of pressure, temperature and velocity in plasma induced during laser ablation of aluminium, 100 ns after the beginning of the laser pulde.

slightly decreases to a value of 3.6×10^4 m $\cdot$ s^{-1}. Further decrease of velocity is very small; the plasma expansion is practically inertial since the drag of residual air is very small.

4. Comparison with experiment

Although aluminium plasma was studied in several papers, it is difficult to find one made in conditions corresponding to our calculations. Available papers describe expansion of Al plume ablated with a lasers working at much higher fluences [21–23]. The fluences were $F = 32$, 165, 90 J $\cdot$ cm^{-2}, respectively and plume velocities varied from 3.5×10^4 m $\cdot$ s^{-1} to 6.5×10^4 m $\cdot$ s^{-1}. Therefore simple experiment was made to enable comparison with the calculations.

An Nd:YAG Quantel YG981 laser was operated at a wavelength of 1064 nm and 10 ns pulse duration. The laser fluence was 10 J $\cdot$ cm^{-2}. The incident angle of the laser beam was 45° to the surface normal. The ablation of an aluminium target was performed in a Pulsed Laser Deposition (PLD) chamber in residual air at a pressure of 1 Pa. The images of the plasma plume were registered with the use of an ICCD camera. The plasma was imaged on the camera using a 180 mm focal length camera lens. The image intensifier was gated for an exposure time of 5 ns while the delay time between the laser pulse and the pulse triggering the image intensifier was changed gradually. The results are shown in Fig. 10.

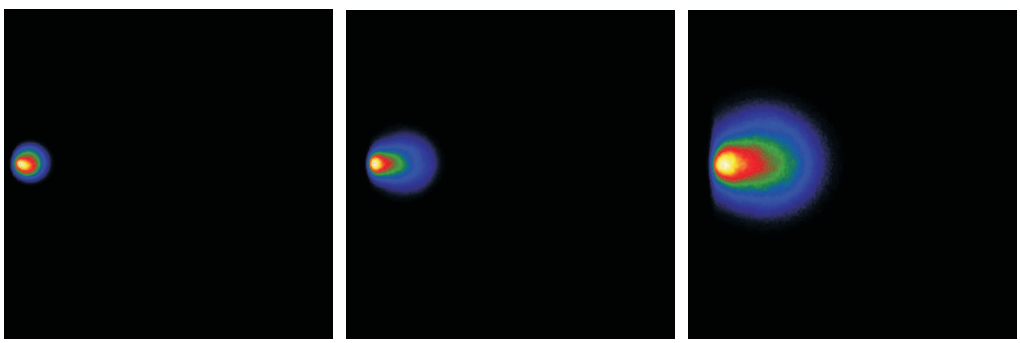

Fig. 10. Images of aluminium plasma images during expansion to residual air at a pressure of 1 Pa. Visible light, exposure time 5 ns, delay time 100, 200 and 300 ns, respectively. Dimensions of the picture 18 $\times$ 18 mm.

The comparison of the experimental plasma shape with the theoretical results is rather difficult because the images show plasma radiation which depends both on plasma density and temperature. However, plasma dimensions are similar; for example, after 100 ns the plasma diameter is about 4 mm. The front velocities obtained from the experimental plasma images amount to $\sim 5 \times 10^4$ m $\cdot$ s^{-1} and are only 25% higher than the calculated front velocities.

5. Conclusions

The model which describes the target heating, formation of the plasma and plasma expansion consists of equations of conservation of mass, momentum and energy and is solved with the use of commercially available program Fluent. The calculations show a sharp increase of the plume temperature and pressure as a result of plasma – laser beam interaction, and following it a considerable increase of the velocity of the plasma plume. The plasma maximum temperature of 61 500 K, maximum pressure of 2×10^8 Pa and a velocity of 3.8×10^4 $\mathrm{m \cdot s^{-1}}$ have been found. It has been shown that the Mie absorption cannot be neglected in the phase of plasma formation and this mechanism can lead to significant increase of the plasma pressure and temperature. The theoretical results are in fair agreement with the experimental observations. The plume velocity obtained from the model is close to that observed in the experiment carried out in similar conditions. This means that high plume velocities observed in experiments can be fully explained by gasdynamic effects and there is no need to include the mechanism of the ions acceleration in the electric field created by the photo- and thermionic electron emission.

Acknowledgements

This paper was supported in part by the research project N N501 069138.

References

1. D Bäuerle, *Laser Processing and Chemistry*, Springer-Verlag, Berlin 1996.
2. V.I Mazhukin, V.V. Nossov, M.G. Nickiforov, I. Smurov, *Optical breakdown in aluminium vapor induced by ultraviolet laser radiation*, J. Appl. Phys., **93**, 56–66, 2003.
3. R.K. Singh, J. Narayan, *Pulsed-laser evaporation technique for deposition of thin films: Physics and theoretical model*, Phys. Rev. B, **41**, 8843–8859, 1990.
4. K.R. Chen, T.C. King, J.H. Hes, J.N. Leboeuf, D.B. Geohegan, B.R.F. Wood, A.A. Puretzky, J.M. Donato, *Theory and numerical modeling of the accelerated expansion of laser-ablated materials near a solid surface*, Phys. Rev. B, **60**, 8373–8382, 1999.
5. T. Nedelea, H.M. Urbassek, *Particle-in-cell simulation of the pulsed planar expansion of a fully ionized plasma off a surface*, Phys. Plasmas, **9**, 3209–3216, 2002.
6. X. Tan, D. Zhang, X. Li, Z. Li, R. Fang, *A new model for studying the plasma plume expansion property during nanosecond pulsed laser deposition*, J. Phys. D: Appl. Phys., **41**, 035210, 2008.
7. Zh. Chen, A. Bogaerts, *Laser ablation of Cu and plume expansion into 1 atm ambient gas*, J. Appl. Phys., **97**, 063305, 2005.
8. V.I. Mazhukin, V.V. Nossov, I. Smurov, *Modeling of plasma-controlled evaporation and surface condensation of Al induced by 1.06 and 0.248 m laser radiations*, J. Appl. Phys., **101**, 024922, 2007.

9. C.J. Knight, *Theoretical modelling of rapid surface vaporization with back pressure*, AIAA J., **17**, 519–523, 1979.

10. FLUENT 6.3. User's Guide.

11. N.M. Bulgakova, A. Bulgakov, L.P. Babich, *Energy balance of pulsed laser ablation: thermal model revised*, Appl. Phys. A, **79**, 1323–1326, 2004.

12. K.C. Mills, *Recommended values of thermophysical properties for selected commercial alloys*, National Physical Laboratory, 2002, UK.

13. J. Richter, *Radiation of hot gases*, [in:] Plasma Diagnostics, W. Lochte-Holtgreven [Ed.], North Holland, Amsterdam 1968.

14. F. Cabannes, J.C. Chapelle, *Reactions Under Plasma Conditions*, M. Venugopalan [Ed.], Wiley-Interscience, New York 1971.

15. J.M. Berger, *Absorption coefficients for free-free transitions in a hydrogen plasma*, Astrophys. J., **124**, 550–554, 1956.

16. G. Weyl, A. Pirri, R. Root, *Laser ignition of plasma off aluminium surfaces*, AIAA J., **19**, 460–469, 1981.

17. H.C. van de Hulst, *Light Scattering by Small Particles*, Dover Publications, New York 1981.

18. L.A. Akashev, V.I. Kononenko, *Optical Properties of Liquid Aluminium and Al-Ce Alloy*, High Temperature, 39, 3, 384–387, 2001.

19. R. Rozman, I. Grabec, E. Govekar, *Influence of absorption mechanisms on laser-induced plasma plume*, Appl. Surf. Sci., **254**, 3295–3305, 2008.

20. H.W. Drawin, P. Felenbock, *Data for Plasmas in Local Thermodynamic Equilibrium*, Gauthier-Villars, Paris 1965.

21. S.S. Harilal, M.S. Tillack, B. O'Shay, C.V. Bindhu, F. Najmabadi, *Confinement and dynamics of laser-produced plasma expanding across a transverse magnetic field*, Phys. Rev., **69**, 026413, 2004.

22. A.K. Sharma, R.K. Thareja, *Plume dynamics of laser-produced aluminum plasma in ambient nitrogen*, Appl. Surf. Sci., **243**, 68–75, 2005.

23. C. Ursu, S. Gurlui, C. Focsa, G. Popa, *Space- and time-resolved optical diagnosis for the study of laser ablation plasma dynamics*, Nucl. Instr. & Methods Phys. Res. B, **267**, 446–450, 2009.

Received May 10, 2010; revised version November 4, 2010.